tions relative to gametes drawn at random from the entire population [S. Wright, *Ann. Eugen.* **15**, 323 (1951)].
4. L. L. Cavalli-Sforza, P. Menozzi, A. Piazza, *History and Geography of Human Genes* (Princeton Univ. Press, Princeton, NJ, in press).
5. C. R. Guglielmino, A. Piazza, P. Menozzi, L. L. Cavalli-Sforza, *Am. J. Phys. Anthropol.* **83**, 57 (1990).
6. C. F. Spoor and P. Y. Sondaar, *J. Hum. Evol.* **15**, 399 (1986).
7. A. Piazza, N. Cappello, E. Olivetti, S. Rendine, *Munibe Antropologia-Arqueologia* **6**, 168 (1988).
8. A. Trombetti, *Le Origini Della Lingua Basca* (Forni, Bologna, 1925).
9. M. Ruhlen, *A Guide to the World's Languages* (Stanford Univ. Press, Stanford, 1987).
10. O. Soffer and C. Gamble, Eds., *The World at 18,000 BP* (Unwin Hyman, London, 1990).
11. P. Menozzi, A. Piazza, L. L. Cavalli-Sforza, *Science* **201**, 786 (1978).
12. R. R. Sokal, N. L. Oden, C. Wilson, *Nature* **351**, 143 (1991); *ibid.* **355**, 214 (1992).
13. A. J. Ammerman and L. L. Cavalli-Sforza, in *The Explanation of Culture Change*, C. Renfrew, Ed. (Duckworth, London, 1973), pp. 343–357.
14. M. Gimbutas, *The Civilization of the Goddess: The World of Old Europe* (Harper, San Francisco, 1991).
15. C. Renfrew, *Archaeology and Language: The Puzzle of Indo-European Origins* (Jonathan Cape, London, 1987).
16. R. R. Sokal, N. L. Oden, B. A. Thomson *Proc. Natl. Acad. Sci. U.S.A.* **89**, 7669 (1992).
17. G. Barbujani and R. R. Sokal, *ibid.* **87**, 1816 (1990).
18. The work described in this Perspective has been supported in part by Consiglio Nazionale delle Ricerche Projects "Genetic Engineering" and "Biological Archive." The color map was produced by S. Rendine with a Computer Grant provided by CSI-Piemonie (Torino, Italy).

ROSAT—A New Look at the X-ray Sky

Joachim Trümper

During the last 30 years x-ray astronomy has become one of the cornerstones of observational astrophysics. At x-ray wavelengths, we see the "hot universe"—objects at temperatures of millions to billions of degrees. We also see large concentrations of relativistic electrons interacting with dense photon fields or magnetic fields. Often the emission of x-rays is connected with explosive events. The brightest objects in the x-ray sky are neutron stars and black holes in the process of accreting matter.

The field of x-ray astronomy has evolved in steps. Major milestones include the 1962 rocket experiment in which the brightest steady x-ray source in the sky was discovered (*1*); the Uhuru satellite, launched in 1971, which was the first astronomy satellite to perform an all-sky survey at x-ray wavelengths (*2*); and the Einstein observatory (1978), the first satellite-borne x-ray telescope, which led to a gain in sensitivity and angular resolution by orders of magnitude (*3*).

A new era of x-ray astronomy began on 1 June 1990 when the German satellite ROSAT was boosted into the sky over Florida by an American rocket. Since then, ROSAT has made a wealth of discoveries on the hot and relativistic matter in our universe. The acronym ROSAT stands for Röentgen Satellite, named after Wilhelm Conrad Röntgen, who discovered x-rays in 1895 in Würzburg and won the first Nobel Prize in Physics in 1901. The satellite was conceived at the Max-Planck-Institut für Extraterrestrische Physik (MPE), which has also taken the scientific lead in this international project (*4*). The satellite comprises two powerful instruments: a large German x-ray telescope sensitive to photon energies from 0.1 to 3 keV and a smaller British extreme ultraviolet (EUV) telescope covering the adjacent band between 25 and 100 eV (Table 1). With these telescopes, the frontiers in x-ray and EUV astronomy could be shifted dramatically.

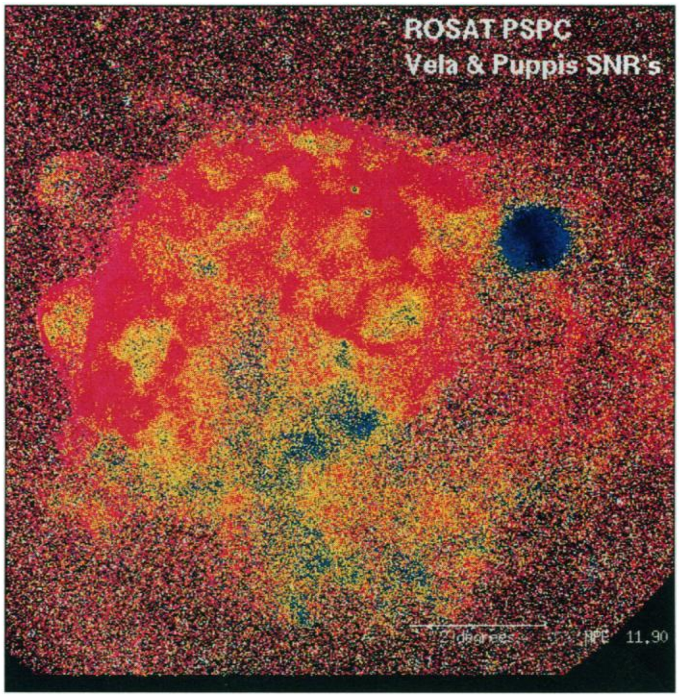

Fig. 1. X-ray shocks. Color map of Vela and Puppis A supernova remnants. Supersonic wakes preceding the main shock front are seen in the east (left), west, and north.

The first half-year of the mission was devoted to an all-sky survey, the first to use imaging x-ray telescopes and the first at all in the EUV. This survey brought a large jump in the number of sources; whereas 840 sources were known from High-Energy Astronomical Observatory 1 (HEAQ-1), a preliminary analysis of the ROSAT survey yielded some 60,000 x-ray sources (*5*) and 384 EUV sources (only a dozen were known before) (*6*). The ROSAT survey includes almost every kind of astrophysical object. The largest classes are active galactic nuclei (>25,000), normal stars (>20,000), clusters of galaxies (~5000), and normal galaxies (a few hundred).

In addition, the x-ray survey revealed the large-scale structure in the sky connected with the distribution of hot and cool gas in our galaxy and some 100 new supernova remnants were found in x-rays (*7*), whereas only about 50 had been known before. Owing to the "unlimited field of view" of the survey, the large galactic structures and old supernova remnants could be mapped as a whole, and the spectral resolution of the image detectors allowed measurement of their temperature distributions for the first time in detail. A special highlight was the discovery of sharp conical structures in supernova remnants (such as Vela) (Fig. 1), indicative of Mach cones produced by clumps of matter moving with Mach numbers of ~3 in the hot interstellar medium.

This enormously productive survey took only half a year. For more than 2 years, ROSAT has been used for detailed observations of selected sources, with some 3400 observations made so far for hundreds of guest observers all over the world. Compared with its famous predecessor, the Einstein observatory, ROSAT imaging offers a substantial increase in sensitivity (factor 3–10), angular resolution (factor 10), spectral resolution (factor 2.5), and imaging quality.

In the well-known Crab nebula, structural features were discovered that reflect the beaming geometry of the Crab pulsar's ultra-relativistic electron and positron wind, which carries particles with energies up to ~10^{14} eV. Several other pulsars were observed at x-ray energies that had been sought for a long time, such as the Vela and Geminga pulsars.

The auhor is director at the Max-Planck-Institut für Extraterrestrische Physik, W-8046, Garching, and is principal investigator of ROSAT at the University of Munich, Germany.

Whereas the Vela pulsar (89-ms period) had been known as a radio, optical, and gamma-ray pulsar, Geminga was just a very bright, mysterious gamma-ray source in the sky. The Geminga pulsar (237 ms) is the first single pulsar discovered at other than radio wavelengths (8). Actually, it has remained undetected in radio, whereas ray pulsations were immediately found with the Compton observatory once the x-ray period was known.

In total, there are now seven single pulsars showing x-ray pulsations. The three youngest ones (Crab, 940 years old; PSR 0540-69, 1660 years old; and PSR 1509-58, 1550 years old) show sharp pulses, a large pulse fraction (nearly 100%), and power-law spectra indicating magnetospheric emission. The three older ones (Vela, 10,000 years old; PSR 0656 + 14, 10^5 years old; and Geminga, 3×10^5 years old) exhibit rather smooth light curves, a small modulation (15%), and spectra consistent with thermal emission from the neutron star surface. Four of these six objects (Crab, PSR 0540-69, PSR 1509-58, and Vela) are surrounded by synchrotron nebulas that are fed by the relativistic winds from their pulsars. The seventh pulsar is a special case: It is the first millisecond pulsar (5.75 ms) for which x-ray pulsations were detected. It is part of a binary system with a 5.75-day period, and the faint optical counterpart (magnitude $m_v = 22$) is probably a white dwarf (9). Millisecond pulsars are believed to be spun-up in binary systems during the mass accretion phase. Such a pulsar must be old, and this is consistent with the spin-down age measured at radio wavelengths of 10^9 years. The x-ray pulsations are smooth and consistent with black-body radiation of 2×10^6 K emitted from a small polar spot on the neutron star surface that must be continuously reheated.

Exciting results have been obtained with ROSAT on nearby galaxies. In Andromeda, 407 sources were found, more than Uhuru saw in the whole sky (*10*). This demonstrates in an impressive way the progress that x-ray astronomy has made during the last 20 years. Of special interest is the ROSAT discovery of a class of sources in nearby galaxies (Andromeda, Large and Small Magellanic Clouds, M101, and M253) characterized by very low temperatures (400,000 K) but luminosities close to the Eddington limit (about 10^{38} erg s^{-1}). These sources are probably white dwarves in binary systems accreting matter at a rate just sufficient to sustain steady nuclear burning on their surfaces and thus represent a long-sought class of sources.

The large collecting power of the ROSAT telescope and the low intrinsic background of the position-sensitive proportional counter (which shows one background count per pixel per day) has allowed the study of diffuse emissions from objects with very low surface brightness, which is important for investigations of galactic halos and clusters of galaxies. The halo of the starburst galaxy NGC 253 has a temperature of 1.6×10^6 K and can be seen out to distances of 10 kpc above the galactic plane (*10*). This giant plasma cloud is produced by winds driven out of the galactic disk by enhanced supernova activity, carrying along magnetic fields and relativistic particles responsible for the radio halo.

Clusters of galaxies are bright, extended x-ray sources representing local density maxima in the universe. The current program of measuring redshifts of a large number of clusters detected in the ROSAT sky survey is therefore of great cosmographical relevance. On the other hand, measurements on nearby objects (Virgo, Coma, Perseus, Abell 2256, and others) show that relaxed clusters of galaxies are the exception rather than the rule. With ROSAT, investigators have found that almost all nearby clusters show structures indicative for interaction processes and merging events (*11*). This gives strong support to hierarchical clustering models.

ROSAT also allowed the measurement of cluster x-ray emission out to about one Abell radius (around 3 Mpc), leading to new determinations of the hot plasma mass and the gravitational (binding) mass of the cluster as well as of the dark matter (*12*). In rich clusters of galaxies (such as Perseus or Coma), the x-ray luminous gas accounts for 10 to 30% of the gravitational mass. For small groups (NGC 2300 or Hickson 62, for instance), values of 5 to 10% might be more typical. In any case, most of the determined gravitational mass of galaxy clusters is still unobserved and one has to recourse to hypothetical forms of "dark matter" for explanation. The large ratio of the mass of the gas to the mass in visible galaxies with values up to a factor of 5 or 6 in rich clusters may indicate, on the other hand, that most of this gas is primordial and there are a lot more baryons in the universe

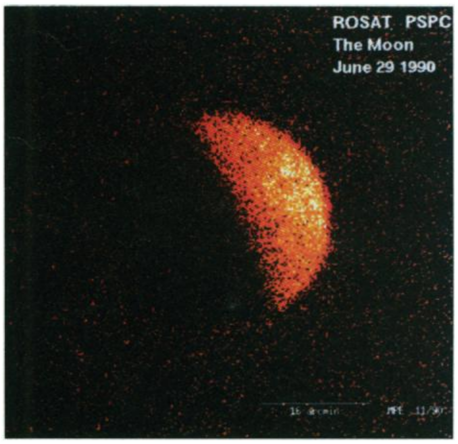

Fig. 2. X-ray moonglow. Image of the moon taken in soft x-ray shows the crescent as well as a distinct x-ray shadow in the diffuse x-ray background cast by the dark side of the moon.

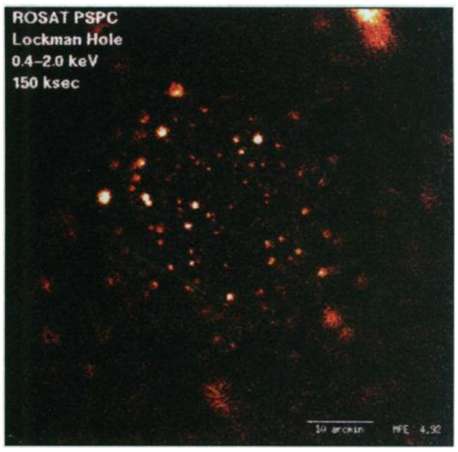

Fig. 3. X-rays of deep space. The deepest observation by ROSAT of a field in Ursa Major had 42 hours of integration time. The image shows the inner part of the ROSAT PSPC field of view. The density of objects in this image is 435 sources per square degree.

Table 1. The international ROSAT collaboration.

Component	Source
Germany	
Satellite	Dornier/MBB
Ground station	German Aerospace Research Establishment (DLR)/GSOC
X-ray mirrors	Carl Zeiss
Focal-plane assembly	MPE Garching
Two-position sensitive proportional counters	MPE Garching
ROSAT Data Center	MPE Garching
German XUV Data Center	Astronomical Institute of Tubingen University
Overall Project Management	DLR-PT/DARA
United Kingdom	
Wide-field camera (XUV telescope)	University of Leicester (leading a consortium of U.K. institutes)
U.K. Project Management	Science and Engineering Research Council (SERC)
United States	
High-resolution imager (x-ray telescope)	Smithsonian Astrophysical Observatory
Launch (Delta-2)	National Aeronautics and Space Administration (NASA)
Ground station backup	NASA
U.S. Project Management	NASA/Goddard Space Flight Center

than we observe in galaxies.

Finally, there are observations that connect ROSAT with the beginnings of x-ray astronomy. The historical rocket flight in 1962 aimed at the detection of x-rays from the moon but discovered the brightest x-ray source (Sco X-1) in the sky and the diffuse x-ray background (*1*). Twenty-eight years later a ROSAT snapshot produced the first x-ray image of the moon (Fig. 2). It shows scattered solar x-rays from the sunlit side and the occultation of the diffuse sky background by the dark side of the moon (*13*). To reveal the nature of this diffuse background—the "holy grail" of x-ray astronomy—the longest ROSAT observation (42 hours) has been made in the constellation Ursa Major (*14*) (Fig. 3). At the source flux level reached (2×10^{-15} erg cm^{-2} s^{-1}, which is a factor of 20 fainter than that of the deepest Einstein survey), 435 sources per square degree show up. At least 75% of the total "background" is resolved into discrete sources. Optical identification shows that most of the brighter sources ($>10^{-14}$ erg cm^{-2} s^{-1}) are quasars with a wide distribution in redshifts. Identification of the faintest ROSAT sources has to await the next generation of optical telescopes, which shall become available soon.

References

1. R. Giacconi *et al.*, *Phys. Rev. Lett.* **9**, 439 (1962).
2. ———, *Astrophys. J.* **165**, L27 (1971).
3. ———, *ibid.* **230**, 540 (1979)
4. J. Trümper, *Adv. Space Res.* **2**, 142 (1983); *Phys. Bl.* **46**, 137 (1990).
5. W. Voges *et al.*, *Proceedings of the European ISY Meeting*, Munich (1992).
6. K. Pounds *et al.*, *Mon. Not. R. Astron. Soc.* **260**, 77 (1993).
7. B. Aschenbach *et al.*, COSPAR *Adv. Space Res.*, in press.
8. J. P. Halpern and S. S. Holt, *Nature* **357**, 222 (1993).
9. W. Becker, J. Trümper, K. T. S. Brazier, T. Belloni, *Int. Aston. Union Circular 5701* (1993).
10. W. Pietsch and J. Trümper, *Adv. Space Res.*, in press.
11. J. P. Henry and U. G. Briel, *ibid.*, in press.
12. H. Böhringer, R. A. Schwartz, U. G. Briel, paper presented at "Observational Cosmology," Milan, 21 to 24 September 1992.
13. J. H. M. M. Schmitt *et al.*, *Nature* **349**, 583 (1991).
14. G. Hasinger *et al.*, *Astron. Astrophys.*, in press.

Natural Selection at Work on the Surface of Virus-Infected Cells

Andrew McMichael

In the last 7 years, considerable progress has been made in understanding how foreign antigens are presented to cytotoxic T lymphocytes (CTLs), a process that enables the CTL to "look inside" other cells and detect abnormalities within, such as a virus infection, and ultimately to destroy the infected cell.

The key element in this recognition of foreign proteins (antigens) by CTLs is the class 1 glycoprotein encoded by the major histocompatibility gene complex (MHC-1). These MHC-1 molecules bind peptide fragments of internal cellular proteins that have been degraded in the cytoplasm (*1*) (see figure). Cytoplasmic proteases, such as those of the proteasome complex, degrade cytoplasmic proteins to peptide fragments. Many of these pieces may be further degraded, but some are taken into the endoplasmic reticulum by a transport mechanism that involves a dimeric protein of the adenosine triphosphate (ATP)–binding cassette family (*2, 3*). (Other members of this family are the cystic fibrosis gene product and the multidrug resistance protein, also involved in transport across cell membranes.) The two chains of the transporter are encoded in the MHC (*2, 3*), as are 2 of the 28 or so subunits of the proteasome (*4*).

The peptides generated and transported into the endoplasmic reticulum are derived from many intracellular proteins. Peptides from viral proteins are mixed into this pool. Some genetic polymorphism in the transporters may influence the type of peptides that reach the lumen of the endoplasmic reticulum (*5*); some viruses may also influence the general composition of this peptide pool by inhibiting host cell protein synthesis. Inside the endoplasmic reticulum, newly synthesized class 1 glycoprotein molecules need peptides to stabilize their folded structure (*6*).

The MHC-1 molecules comprise two chains, the α (heavy) chain of 45 kilodaltons and a light chain, β_2-microglobulin. The former is the product of the MHC and is uniquely polymorphic. The MHC-1 α chains are encoded by genes at three loci—in humans *HLA-A*, *-B*, and *-C*. There are at least 40 alleles at A, 80 at B, and about 10 at C (*7*). (As more ethnic groups are studied, more alleles are being found, often differing in only a few amino acids from previously sequenced molecules.) HLA-A and HLA-B are expressed at much higher levels than HLA-C and are found on the surface of most nucleated cells. The structures of four MHC-1 molecules, HLA-A2, HLA-A68, HLA-B27, and H-2K^b have been determined (*8*); all are closely related, and on the surface of the molecule that is farthest from the cell membrane is a groove that contains a peptide, 8 to 11 amino acids in length (*9*). Identical MHC-1 molecules on a cell bind many different peptides: the 10^5 HLA-A2 molecules on lymphocytes bind about 10^3 different peptides (*10*). When the mature MHC-1 peptide complex reaches the cell surface, the bound peptides are displayed for many hours; some empty molecules can reach the cell surface but tend to be unstable and fall apart (*11*).

Most of the polymorphism in MHC-1 molecules is found in amino acids with side chains that contribute to the peptide-binding groove (*12*). Thus, the groove of different allelic products differs in its fine structure and binds different peptides. However, the ends of the groove are remarkably conserved, and invariant tyrosines and threonines form hydrogen bonds with the amino-end carboxyl termini of the peptides, so that all peptides bind with the same orientation (*13*). When the bound peptides are eluted from the purified MHC-1 molecules and sequenced, they show similarities at the residues that are involved in binding to the groove (*14*). For instance, in peptides that bind to HLA-B27 there is invariably an arginine at its second residue, often followed by an aromatic residue at position three and an arginine or lysine at the carboxyl terminus (*15*). This is explained by the way the peptides bind to the HLA-B27 molecule; the side chain of the arginine-2 fits into a pocket with features unique to HLA-B27, and the other anchoring side chains also fit into pockets within the groove. Other MHC-1 molecules require different characteristics in their bound peptides. Therefore, different allelic products of the MHC-1 loci present different families of peptides at the cell surface. Among these will be abnormal or foreign peptides if the cell is damaged (for example, by abnormal expression of oncogenes) or infected with a virus, bacterium, or protozoal parasite.

CTLs are crucial for the immune response to viral infections (*16*). They cannot neutralize free virus, but by eliminating virus-infected cells they are often largely responsible for the recovery of the organism from the viral infection (*17*). CTLs are designed to monitor the MHC-1 molecules of cells within the body; if the antigen receptors (also called T cell receptors) on the T cells are bound by antigen, the T cells are activated and they kill the target cells. As CTLs develop in the thymus, those with T cell receptors that react with self peptide–MHC-1 complexes are eliminated (negative selection) or

The author is in the Molecular Immunology Group, Institute of Molecular Medicine, John Radcliffe Hospital, Headington, Oxford OX3 9DU, United Kingdom.